Proc. Natl. Acad. Sci. USA
Vol. 93, pp. 2735–2740, April 1996
Biochemistry

Structural basis for specificity and potency of a flavonoid inhibitor of human CDK2, a cell cycle kinase

(cyclin-dependent kinase/protein kinase inhibitors/cancer/drug design/flavopiridol)

WALTER FILGUEIRA DE AZEVEDO, JR.*, HANS-JOACHIM MUELLER-DIECKMANN*, URSULA SCHULZE-GAHMEN*, PETER J. WORLAND†, EDWARD SAUSVILLE†, AND SUNG-HOU KIM*‡

*Department of Chemistry and Lawrence Berkeley National Laboratory, University of California, Berkeley, CA 94720; and †Laboratory of Biological Chemistry, Developmental Therapeutics Program, Division of Cancer Treatment, National Cancer Institute, Bethesda, MD 20892

Contributed by Sung-Hou Kim, December 8, 1995

ABSTRACT **The central role of cyclin-dependent kinases (CDKs) in cell cycle regulation makes them a promising target for studying inhibitory molecules that can modify the degree of cell proliferation. The discovery of specific inhibitors of CDKs such as polyhydroxylated flavones has opened the way to investigation and design of antimitotic compounds. A novel flavone, (-)-*cis*-5,7-dihydroxyphenyl-8-[4-(3-hydroxy-1-methyl)piperidinyl]-4*H*-1-benzopyran-4-one hydrochloride hemihydrate (L868276), is a potent inhibitor of CDKs. A chlorinated form, flavopiridol, is currently in phase I clinical trials as a drug against breast tumors. We determined the crystal structure of a complex between CDK2 and L868276 at 2.33-Å resolution and refined to an R_{factor} of 20.3%. The aromatic portion of the inhibitor binds to the adenine-binding pocket of CDK2, and the position of the phenyl group of the inhibitor enables the inhibitor to make contacts with the enzyme not observed in the ATP complex structure. The analysis of the position of this phenyl ring not only explains the great differences of kinase inhibition among the flavonoid inhibitors but also explains the specificity of L868276 to inhibit CDK2 and CDC2.**

Cell cycle progression is tightly controlled by the activity of cyclin-dependent kinases (CDKs) (1–3). CDKs are inactive as monomers, and activation requires binding to cyclins, a diverse family of proteins whose levels oscillate during the cell cycle, and phosphorylation by CDK-activating kinase (CAK) on a specific threonine residue (4, 5). In addition to the positive regulatory role of cyclins and CAK, many negative regulatory proteins (CDK inhibitors, CKIs) have been discovered (6), such as p16 (7–9), p21 (10–13), and p28 (14). Since deregulation of cyclins and/or alteration or absence of CKIs have been associated with many cancers, there is strong interest in chemical inhibitors of CDKs that could play an important role in the discovery of new family of antitumor agents.

L868276 is a flavone with a novel structure (Fig. 1), compared to that of polyhydroxylated flavones, including quercetin or genistein (15). Previous studies have shown that flavopiridol, a flavonoid, can inhibit growth of breast and lung carcinoma cell lines and can inhibit CDK activity at the same nanomolar concentration range of the inhibitor (16). To understand how flavopiridol analogs bind to CDK2, we determined the x-ray structure of CDK2 in complex with the *des*-chloroflavopiridol L868276 and compared it with the x-ray structure of the CDK2–ATP complex (17).

MATERIALS AND METHODS

Human CDK2 was prepared as described (18). In brief, Sf9 insect cells were infected with baculovirus containing the human CDK2 gene. The supernatant of cell lysate was loaded over a DEAE-Sepharose column followed by an S-Sepharose column. The flowthrough was loaded onto an ATP affinity column and eluted by a NaCl gradient. The purified protein is fully functional in assays of CDK2 activation *in vitro*: it binds with high affinity to human cyclin A *in vitro*, and the resulting complex can be fully activated when incubated with partially purified human CAK.

L868276 is derived by chemical synthesis from a parent structure obtained from *Dysoxylum binectariferum* (16), a plant native to India. L868276 can be obtained from Harald Sedlacek, Behringwerke, Marburg, Germany.

Inhibitor Soaking and Cocrystals. We crystallized CDK2 in the conditions described earlier (18). In brief, a CDK2 solution was concentrated to 10 mg/ml by dialysis against 20 mM Hepes buffer (pH 7.4) with 1 mM EDTA. Sitting drops were equilibrated by vapor diffusion at 4°C against reservoirs containing 200 mM Hepes buffer at pH 7.4. Diamond and wedge-shaped crystals appeared after 2–4 days. A gradual increase of the Hepes concentration in the reservoirs (up to 800 mM) produced crystals with average dimensions of about 0.2 mm × 0.3 mm × 0.3 mm. After CDK2 crystals had formed, small amounts of L868276 powder were added to the crystallization drops by using a cat whisker. Most of the crystals cracked after a few days, possibly indicating binding of the inhibitor to CDK2. Addition of smaller amounts of inhibitor to the crystallization drops prevented the crystals from cracking. Crystals were soaked for 48 hr before data collection. Cocrystallization experiments using the crystallization conditions for CDK2 as well as the sparse matrix method (19) were also undertaken, but thus far we have not obtained any x-ray-diffracting cocrystals. Preliminary x-ray studies showed that the soaked crystals diffracted to 2.3 Å, although they decayed quickly when exposed to x-rays at room temperature. To overcome this difficulty we collected data from a flash-frozen crystal at 100 K. Prior to flash freezing, 2-methyl-2,4-pentanediol (MPD) was added, up to 30% by volume, to the crystallization drops for cryoprotection. The crystals were of the same space group as the apoenzyme and the CDK2–ATP crystals. Upon freezing the cell parameters shrank from a = 73.12 Å, b = 72.72 Å, and c = 54.25 Å to a = 71.30 Å, b = 72.03 Å, and c = 53.70 Å.

Data Collection and Structure Refinement. X-ray diffraction data for the CDK2–L868276 complex crystal were collected with a Rigaku R-AXIS-II imaging plate area detector and processed with the RAXIS data processing software (Table 1). Attempts to refine the position of the CDK2–apoenzyme model as a rigid body against the CDK2–L868276 complex data by using X-PLOR 3.0 (20) were unsuccessful. The R_{factor} of the CDK2–L868276 complex decreased from 52.3% to 46.7% with data from 8.0 Å to 3.0 Å, indicating that the CDK2–L868276 frozen crystal has a packing arrangement different from that of the CDK2–apoenzyme crystal. We did not expect

The publication costs of this article were defrayed in part by page charge payment. This article must therefore be hereby marked "*advertisement*" in accordance with 18 U.S.C. §1734 solely to indicate this fact.

Abbreviation: CDK, cyclin-dependent kinase.

‡To whom reprint requests should be addressed.

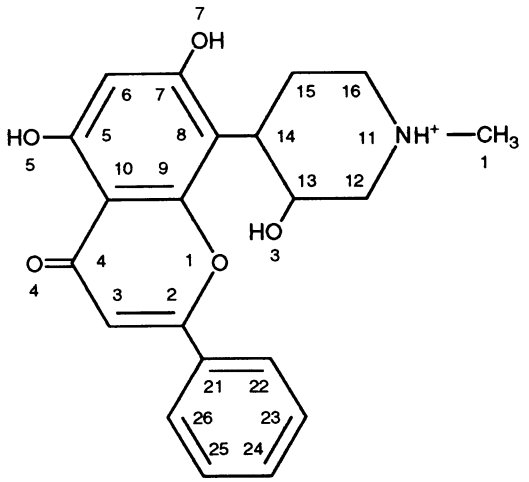

FIG. 1. Molecular structure of (-)-*cis*-5,7-dihydroxyphenyl-8-[4-(3-hydroxy-1-methyl)piperidinyl]-4*H*-1-benzopyran-4-one hydrochloride hemihydrate (L868276).

major differences between the structures of CDK2–L868276 and CDK2–apoenzyme, since the CDK2–L868276 complex was obtained by soaking L868276 into the apoenzyme crystals. Hence, instead of using the standard procedure of complete molecular replacement, we performed only a translational search in X-PLOR 3.0, skipping the rotational search and the PC refinement (20). We also restricted the translational search to a small part of the cell from -0.05 to 0.05 in x, y, and z, in fractional coordinates, instead of scanning half of x, y, and z as described by Hirshfeld (21) for the space group $P2_12_12_1$. The highest peak in fractional coordinates was at $x = -0.036$, $y = -0.007$, $z = -0.007$. In the following rigid-body refinement the R_{factor} decreased from 33.4% to 31.2% for the data between 8.0 Å and 3.0 Å. At this stage $F_o - F_c$ maps were calculated. These maps showed clear density for inhibitor bound to the ATP-binding pocket of CDK2.

The conformation of residues forming the ATP-binding pocket was checked in simulated annealing omit maps before the inhibitor molecule was included in the complex structure. Further refinement in X-PLOR continued with simulated annealing using the slow-cooling protocol (22), followed by alternate cycles of positional refinement and manual rebuilding using FRODO (23). Finally, the positions of water molecules were checked and corrected in $F_o - F_c$ omit maps. Water molecules were modeled into difference densities larger than 3σ. The final model has an R_{factor} of 20.3% and an R_{free} of 28.8% with good stereochemistry (Table 2).

Root-mean-square (rms) differences from ideal geometries for bond lengths and angles were calculated with X-PLOR 3.0 (20). Protein superpositions based on C^α atoms were done with the program LSQKAB from CCP4 (24). Hydrogen bonds and van der Waals contacts were assigned with the program CONTACSYM (25). The cutoff for hydrogen bonds and salt bridges was 3.4 Å, and up to 4.11 Å for van der Waals contacts, depending on the atom type, and using standard van der Waals radii. The solvent accessibility of individual residues was assessed with the program MS (26) using a 1.7-Å radius for the solvent probe.

Table 1. Diffraction data collection statistics of CDK2 complex with L868276

Space group	$P2_12_12_1$
Cell dimensions, Å	$a = 71.30$
	$b = 72.03$
	$c = 53.70$
No. of measurements $[I/\sigma(I)>1.0]$	35,891
No. of unique reflections	11,430
Completeness of data to 2.33 Å, %	91.7
R_{sym},* %	4.9

*$R_{sym} = 100 \times \Sigma|I(h) - \langle I(h)\rangle|/\Sigma I(h)$, with $I(h)$, observed intensity and $\langle I(h)\rangle$, mean intensity of reflection h over all measurements of $I(h)$.

Table 2. Refinement statistics for CDK2 complex with L868276

Resolution, Å	8.00–2.33
R_{factor},* %	20.3
R_{free},† %	28.8
B values,‡ Å^2	
Main chain	31.0
Side chains	33.7
Inhibitor	34.4
Waters	37.0
Deviations observed	
rms, bond lengths, Å	0.012
rms, bond angles, degrees	1.7
No. of water molecules	84

*$R_{factor} = 100 \times \Sigma|F_o - F_c|/\Sigma(F_o)$, the sums being taken over all reflections with $F/\sigma(F) > 2$ cutoff.
†$R_{free} = R_{factor}$ for 10% of the data, which were not included during crystallographic refinement.
‡B values = average B values for all non-hydrogen atoms.

RESULTS

Overall Protein Conformation. The CDK2 portion of the CDK2–L868276 complex structure is almost identical to the CDK2 structure found in CDK2–apoenzyme (17), ATP complex (17), olomoucine complex (27), and isopentenyladenine complex (27) and very similar to that in CDK2–cyclin A complex (28). As observed in several of the CDK2 structures, electron density is weak in two regions in the enzyme, spanning residues 36–47 and 150–164. The Ramachandran plot (29) for the L868276 inhibitor complex shows tight clustering of peptide conformation in the energetically favorable regions.

The enzyme is folded into the typical bilobal structure, with the smaller, N-terminal domain consisting predominantly of β-sheet structure and the larger, C-terminal domain consisting primarily of α-helices. There are no significant differences in the domain orientations between the inhibitor–enzyme complex and the ATP–enzyme complex. The inhibitor binds, as seen for ATP and the adenine derivative inhibitors, in the deep cleft between the two domains (Fig. 2). Positional differences for C^α atoms between the CDK2–L868276 complex and the CDK2–ATP complex range from 0.06 Å to 3.35 Å, with an average displacement of 0.46 Å. The highly flexible regions (residues 36–47 and 150–164) were excluded from these calculations. The largest rms differences are mainly observed in the N-terminal 30 residues in β-strands 1 and 2, which form a part of the ATP-binding pocket provided by the small domain. The average displacement of C^α atoms in this region is 0.75 Å.

Conformation of Bound L868276 and the Ligand-Binding Pocket. The electron density for most atoms of the inhibitor L868276 is clear and strong (Fig. 3*a*). L868276 binds in the ATP-binding pocket, with the benzopyran ring of L868276 occupying approximately the same region as the purine ring of ATP (Fig. 3*b*). The two ring systems overlap in the same plane, but the benzopyran in L868276 is rotated about 60° relative to the adenine in ATP, measured as the angle between the carbon–carbon bonds joining the two cycles in benzopyran and adenine rings, respectively (Fig. 3*c*). In this orientation, the O5 hydroxyl and the O4 of L868276 are close to the positions of the N6 amino group and N1 in adenine, respectively. In the L868276 molecule the phenyl ring is pointing toward the outside of the ATP-binding pocket and occupies a region not occupied by any parts of the ATP in the ATP complex. The piperidinyl ring partially occupies the α-phosphate pocket and

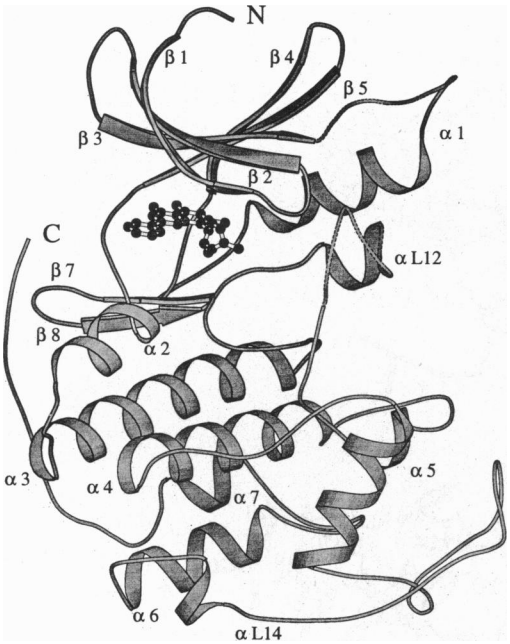

FIG. 2. Schematic drawing of CDK2 with the inhibitor L868276 in the ATP-binding pocket between the smaller, N-terminal domain and the larger, C-terminal domain. Secondary structural elements are indicated by arrows for β-strands and coils for α-helices and are labeled as in the apoenzyme (17). Residues 36–47 and 150–164, which have weak electron densities, are drawn with dotted lines.

is assigned to a chair conformation, although a boat conformation cannot be ruled out completely.

In the ATP complex structure (17), CDK2 interactions with ATP are characterized by predominantly hydrophobic and van der Waals interactions between the protein and the adenine base, and ionic interactions, hydrogen bonds, and van der Waals interactions with the ribose and triphosphate of ATP (Fig. 4*a*). In total, there are 26, 15, and 38 contacts between CDK2 and the adenine base, ribose, and phosphates, respectively. The adenine ring is enclosed in a hydrophobic pocket formed by Ile^{10}, Ala^{31}, Val^{64}, Phe^{80}, Phe^{82}, and Leu^{134} (Fig. 4*a*) and forms two hydrogen bonds, between the N6 atom of the adenine and the carbonyl oxygen of Glu^{81}, and between N1 and the backbone amide of Leu^{83}. The same hydrogen bonds are conserved in the cyclic AMP-dependent kinase (PKA) structure (30, 31), and the bond to N6 has been shown to be important for binding affinity (32).

In the L868276 complex structure, the inhibitor molecule is quite hydrophobic. Hence, binding to CDK2 is characterized by predominantly hydrophobic and van der Waals interactions with the same hydrophobic enzyme residues that form the pocket for the adenine base in the ATP complex structure. However, there are more contacts between the enzyme and the benzopyran ring of L868276 (34 contacts) than were seen between the enzyme and the adenine ring of ATP (26 contacts) (Fig. 4 *a* and *b*). We observed 5 hydrogen bonds between L868276 and the enzyme, involving Lys^{33}, Glu^{81}, Leu^{83}, and Asp^{145}, residues that also form hydrogen bonds in the ATP complex. There are 7 van der Waals contacts with the hydroxymethyl piperidinyl ring, and 10 with the phenyl ring, which increase the total number of contacts between L868276 and CDK to 56. Many of the contacts between L868276 and CDK2 are made by only three residues, Ile^{10}, Leu^{83} and Leu^{134}, which form a total of 24 contacts (Fig. 4*b*), corresponding to 43% of the observed contacts. Two of the CDK2 residues in contact with phenyl ring, His^{84} and Lys^{89}, are unique to the CDK2–L868276 complex.

Geometric Complementarity and Buried Surface Areas. The specificity and affinity between a protein and its cognate ligand depend on directional hydrogen bonds and ionic interactions, as well as on shape complementarity of the contact surfaces of both partners (33, 34). The shape complementarity is best described as solvent-accessible surfaces that become buried upon ligand binding. If the complementarity is good, the size of the buried areas in a protein and its cognate ligand should be similar. In the CDK2–ATP complex, the buried areas of ATP (352 $Å^2$) and CDK2 (435 $Å^2$) show a close fit. ATP is almost completely inaccessible to solvent and its buried surface amounts to 80% of the buried surface in CDK2. Corresponding values are 301 $Å^2$ and 399 $Å^2$ for L868276 and CDK2, respectively, and the buried surface for L868276 amounts to 75% of the buried surface in CDK2. Much smaller buried surfaces have been reported for adenine derivative inhibitors (27).

Differences in Protein Side-Chain Conformations in the Binding Pocket. To find out whether L868276 binding to CDK2 induces changes in side-chain conformation in the binding pocket, we compared the binding pockets of the CDK2–L868276 complex and the CDK2–ATP complex after a superposition of the enzymes based on their C^α atoms (Fig. 3*b*). This superposition revealed the significant movement of few side chains. Asp^{145} changed its position in the L868276 complex, with C^γ moving by 2.66 Å away from its position in the ATP complex. The preceding residue, Ala^{144}, changes its position by moving closer to the ligand in the L868276 complex. The side chain of Lys^{89} is moved away from the binding pocket. The $N\zeta$ atom moves by 2.54 Å relative to the ATP complex structure and makes two contacts with the phenyl ring in the L868276 complex. In summary, the L868276 inhibitor fits very well to the binding pocket with small adjustments in the side chains. Conformational differences in a few other side chains in the binding pocket are probably not significant, since high temperature factors and weak or missing electron densities indicate high flexibility for those residues.

DISCUSSION

The high-resolution x-ray structure of human CDK2 in complex with a flavopiridol analog, L868276, provides the structural basis for understanding the specificity and potency of this inhibitor compared with other inhibitors as well as the protein's authentic ligand, ATP. Especially interesting is the region of CDK2 occupied by the phenyl ring of the L868276 molecule that is pointing away from the ATP-binding pocket (Fig. 3*b*). This region is not occupied by any parts of the ATP molecule in the ATP complex but contributes with 10 van der Waals contacts to the phenyl ring of the inhibitor in the L868276 complex. The main contact residues are Leu^{83}, His^{84}, and Asp^{86}. The position of the phenyl ring of L868276 is also responsible for the different position of the side chain of residue Lys^{89} (Fig. 3*b*), which is moved away from the binding pocket in the L868276 complex.

The flavopiridol molecule currently in clinical trials has a chlorophenyl instead of the phenyl in the L868276 molecule, and this modification increases the kinase inhibition by a factor of 6 (35). This is probably due to the new possible contacts that the chlorine makes with residues Leu^{10}, Phe^{82}, and Leu^{83}, increasing the total number of contacts between flavopiridol and enzyme to 61. The observation that when the phenyl group is replaced by an ethyl or propyl group, the potency goes down by a factor of >6 (35) can also be understood from the poor interaction of these groups with the protein at this region. The crystal structure of the complex suggests a few positions of L868276 for potential modifications to improve kinase inhibition.

CDC2 and CDK2 kinase activity is potently inhibited by flavopiridol (IC_{50} = 0.40 μM). In contrast, flavopiridol has not

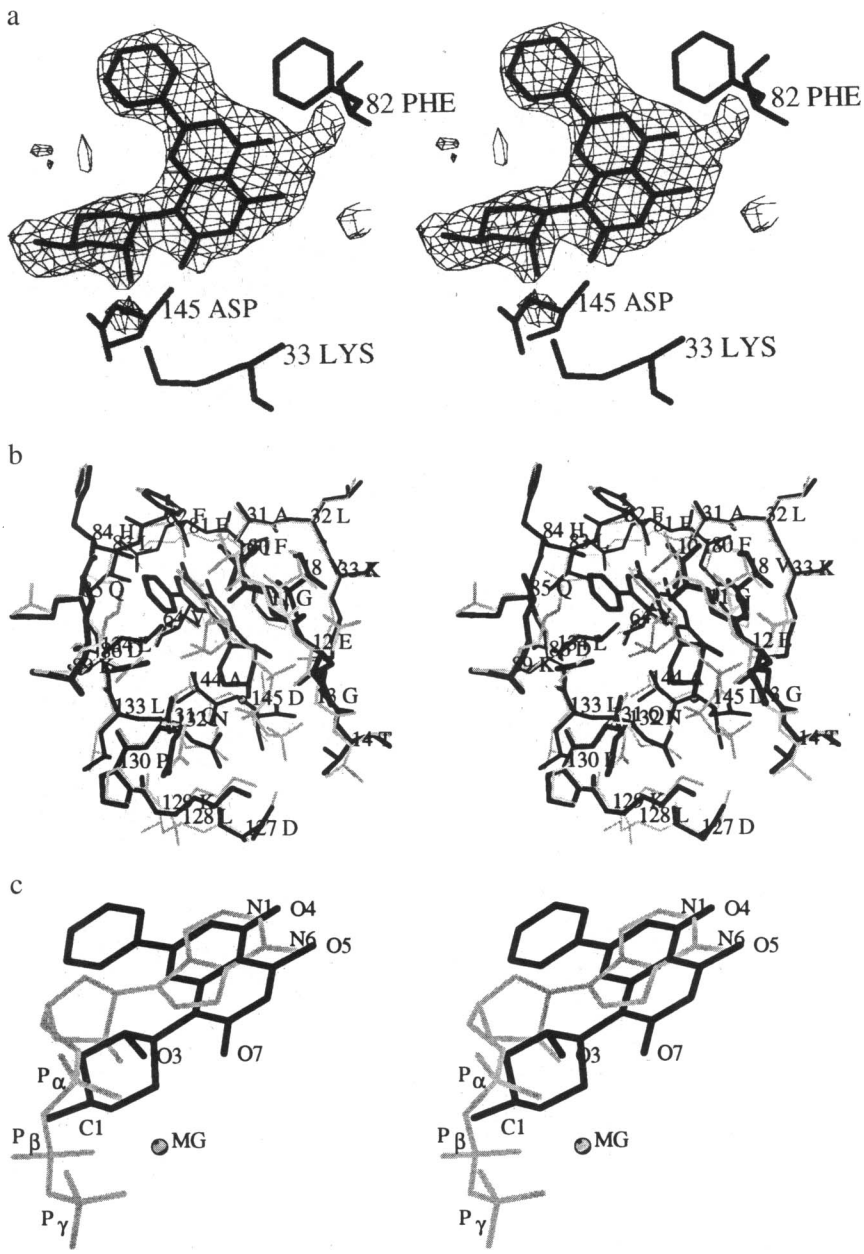

FIG. 3. Stereoviews. (*a*) Electron density for L868276 in difference electron density maps calculated after simulated annealing refinement. The maps are contoured at 2.5σ and displayed with FRODO (23). (*b*) Superimposed binding pockets of CDK2–ATP complex and CDK2–L868276 complex. The ATP complex is shown in gray. The L868276 is drawn in black. (*c*) CDK2 ligands after superposition of the complex structures on C^{α} atoms of CDK2.

been shown to inhibit as potently other protein kinases, such as cyclic AMP-dependent protein kinase (PKA) (IC_{50} = 145 μM) (15). This can be understood by a comparison of the residues that make contact with L868276 in the CDK2–L868276 structure with the equivalent residues in the other kinases: The major differences between CDK2, CDC2, and PKA occur in the residues of CDK2 that make contacts with the phenyl ring of L868276 inhibitor (Ile^{10}, Leu^{83}, His^{84}, Asp^{86}, and Lys^{89}). In CDC2, which is potently inhibited by flavopiridol, these residues are almost completely conserved as Ile^{10}, Leu^{83}, Ser^{84}, Asp^{86}, and Lys^{89}. In contrast, in PKA, which is not potently inhibited, no residue is conserved. We used the numbering scheme shown in ref. 17 for CDK2 and CDC2 sequences, and the numbering scheme adopted for the PKA sequence was taken from ref. 36.

In summary, the comparison of the three-dimensional structures of the CDK2–L868276 complex with the CDK2–ATP complex shows that the hydrophobic adenine-binding pocket has a surprising ability to accommodate molecular structures that are completely different from adenine derivatives. Furthermore, specificity of the inhibitor for the cell cycle kinases over non-cell-cycle kinases can be obtained by a moiety such as phenyl group interacting on a protein surface outside of the ligand-binding pocket. This discovery opens the possibility of testing new inhibitor families, in addition to new substituents for the already known lead structures such as flavone and adenine derivatives.

This work has been supported by a fellowship to W.F.A. from the Conselho Nacional de Pesquisas (Brazil) and by grants from the Office of Health and Environmental Research, U.S. Department of Energy (DE-AC03-76SF00098), and National Institutes of Health.

1. Norbury, C. & Nurse, P. (1992) *Annu. Rev. Biochem.* **61,** 441–470.
2. Fang, F. & Newport, J. W. (1991) *Cell* **66,** 731–742.

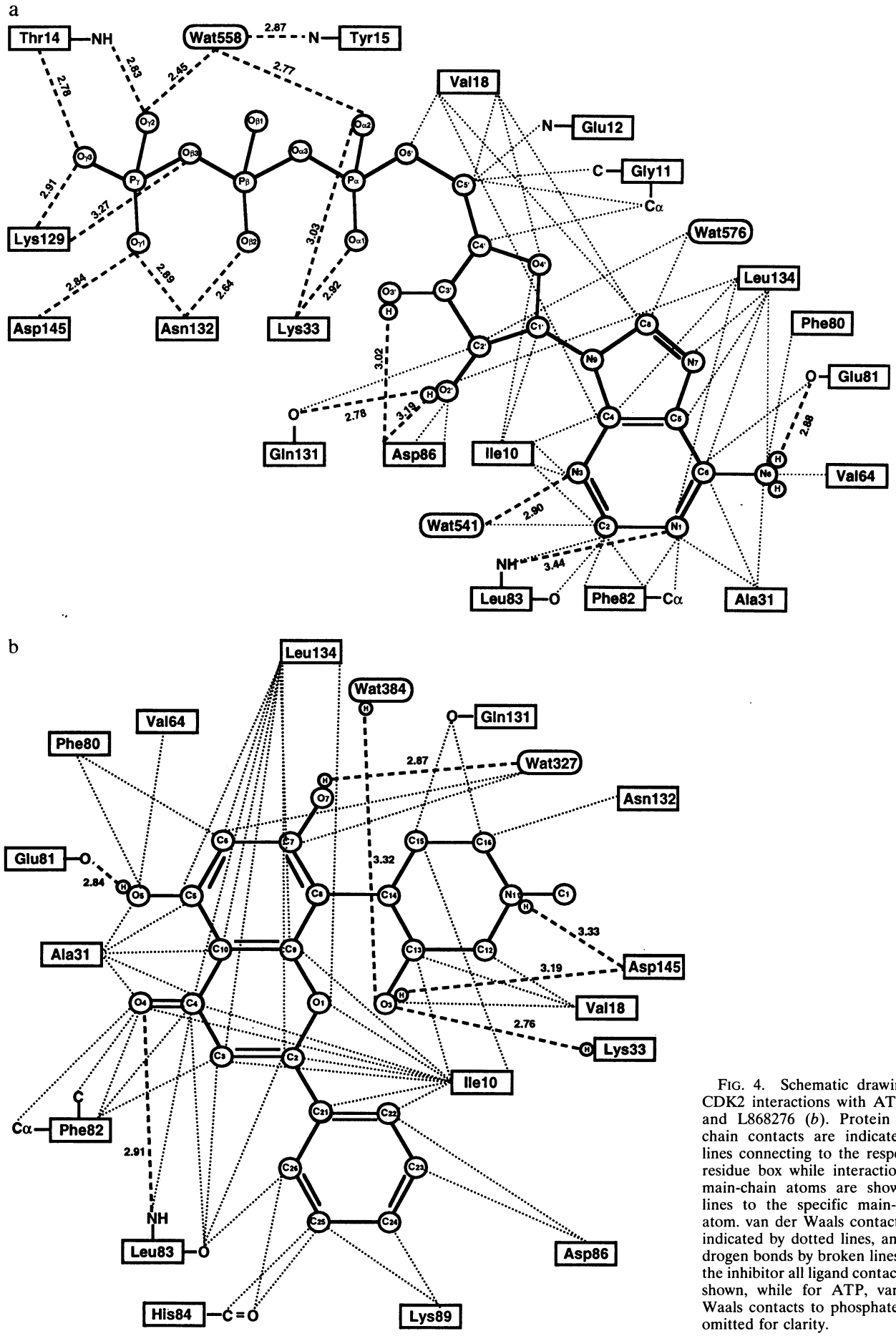

FIG. 4. Schematic drawing of CDK2 interactions with ATP (*a*) and L868276 (*b*). Protein side-chain contacts are indicated by lines connecting to the respective residue box while interactions to main-chain atoms are shown as lines to the specific main-chain atom. van der Waals contacts are indicated by dotted lines, and hydrogen bonds by broken lines. For the inhibitor all ligand contacts are shown, while for ATP, van der Waals contacts to phosphates are omitted for clarity.

3. Hunt, T. (1989) *Curr. Opin. Cell Biol.* **1,** 274–286.
4. Desai, D., Gu, Y. & Morgan, D. O. (1992) *Mol. Biol. Cell* **3,** 571–582.
5. Gu, Y., Rosenblatt, J. & Morgan, D. O. (1992) *EMBO J.* **11,** 3995–4005.
6. Richardson, H. E., Stueland, C. S., Thomas, J., Russel, P. & Reed, S. I. (1990) *Genes Dev.* **4,** 1332–1344.
7. Serrano, M., Hannon, G. J. & Beach, D. (1993) *Nature (London)* **366,** 704–707.
8. Peter, M. & Herskowitz, I. (1994) *Cell* **79,** 181–184.
9. Nobori, T., Miura, K., Wu, D. J., Lois, A., Takabayashi, K. & Carson, D. A. (1994) *Nature (London)* **368,** 753–756.
10. Gu, Y., Turck, C. W. & Morgan, D. O. (1993) *Nature (London)* **366,** 707–710.
11. Xiong, Y., Hannon, G. J., Zhang, H., Casso, D., Kobayashi, R. & Beach, D. (1993) *Nature (London)* **366,** 701–704.
12. Harper, J. W., Adami, G. R., Wei, N., Keyomarsi, K. & Elledge, S. J. (1993) *Cell* **75,** 805–816.
13. Dulic, V., Kaufmann, W. K., Wilson, S. J., Tisty, T. D., Lees, E., Harper, J. W. & Elledge, S. J. (1994) *Cell* **76,** 1013–1023.
14. Hengst, L., Dulic, V., Slingerland, J. M., Lees, E. & Reed, S. I. (1994) *Proc. Natl. Acad. Sci. USA* **91,** 5291–5295.
15. Losiewicz, M. D., Bradley, A. C., Kaur, G., Sausville, E. A. & Worland, P. J. (1994) *Biochem. Biophys. Res. Commun.* **201,** 589–595.
16. Kaur, G., Stetler-Stevenson, M., Seber, S., Wordland, P., Sedlacek, H., Myers, C., Czech, J., Naik, R. & Sausville, E. (1992) *J. Natl. Cancer Inst.* **84,** 1736–1740.
17. De Bondt, H. L., Rosenblatt, J., Jancarik, J., Jones, H. D., Morgan, D. O. & Kim, S.-H. (1993) *Nature (London)* **363,** 595–602.
18. Rosenblatt, J., De Bondt, H., Jancarick, J., Morgan, D. O. & Kim, S.-H. (1993) *J. Mol. Biol.* **230,** 1317–1319.
19. Jancarik, J. & Kim, S.-H. (1991) *J. Appl. Crystallogr.* **24,** 409–411.
20. Brünger, A. T. (1991) X-PLOR, A System for Crystallography and NMR (Yale Univ. Press, New Haven, CT), Version 3.0.
21. Hirshfeld, F. L. (1968) *Acta Crystallogr.* **A24,** 301–311.
22. Brünger, A. T. & Krukowski, A. (1990) *Acta Crystallogr.* **A46,** 585–593.
23. Jones, T. A. (1978) *J. Appl. Crystallogr.* **23,** 434–436.
24. Collaborative Computational Project, No. 4 (1994) *Acta Crystallogr.* **D50,** 760–763.
25. Sheriff, S., Hendrickson, W. A. & Smith, J. L. (1987) *J. Mol. Biol.* **197,** 273–296.
26. Connolly, M. L. (1983) *J. Appl. Crystallogr.* **16,** 548–558.
27. Schulze-Gahmen, U., Brandsen, J., Jones, H. D., Morgan, D. O., Meijer, L., Vesely, J. & Kim, S.-H. (1995) *Proteins Struct. Funct. Genet.* **22,** 378–391.
28. Jeffrey, P. D., Russo, A. A., Polyak, K., Gibbs, E., Hurwitz, J., Massagué, J. & Pavletich, N. P. (1995) *Nature (London)* **376,** 313–320.
29. Ramachandran, G. N., Venkatchalam, C. M. & Krimm, S. (1966) *Biophys. J.* **6,** 849–872.
30. Zheng, J., Knighton, D. R., Ten Eyck, L. F., Karlsson, R., Xuong, N.-H., Taylor, S. S. & Sowadski, J. M. (1993) *Biochemistry* **32,** 2154–2161.
31. Bossemeyer, D., Engh, R. A., Kinzel, V., Ponstingl, H. & Huber, R. (1993) *EMBO J.* **12,** 849–859.
32. Hoppe, J., Freist, W., Marutzky, R. & Shaltiel, S. (1978) *Eur. J. Biochem.* **90,** 427–432.
33. Janin, J. & Chothia, C. (1990) *J. Biol. Chem.* **265,** 16027–16030.
34. Wilson, I. A. & Stanfield, R. L. (1993) *Curr. Opin. Struct. Biol.* **3,** 113–118.
35. Losiewicz, M. D., Carlson, B. A., Sausville, E. A., Nauk, R. G., Narayanan, V. L. & Worland, P. J. (1995) Proceedings of the 88th Annual Meeting of American Association for Cancer Research (Toronto, Canada), Vol. 36, p. 35 (abstr.).
36. Serota, S. & Radzio-Andzelm, E. (1994) *Structure* **2,** 345–355.